Relation between magnetization and Faraday angles produced by ultrafast spin-flip processes within the three-level Λ-type system

Y. Hinschberger, and J. P. Lavoine

Articles you may be interested in

Laser-induced ultrafast demagnetization time and spin moment in ferromagnets: First-principles calculation
Journal of Applied Physics **117**, 17D706 (2015); 10.1063/1.4907693

Perspective: Ultrafast magnetism and THz spintronics
Journal of Applied Physics **120**, 140901 (2016); 10.1063/1.4958846

Relation between magnetization and Faraday angles produced by ultrafast spin-flip processes within the three-level Λ-type system

Y. Hinschberger[1] and J. P. Lavoine[2]

[1]*Departamento de Física e Astronomia, Instituto de Física dos Materiais da Universidade do Porto, Rua do Campo Alegre, 687, 4169-007 Porto, Portugal*
[2]*Departement of Ultrafast Optics and Nanophotonics, Institut de Physique et Chimie des Matériaux de Strasbourg, UMR 7504, CNRS, Université de Strasbourg, 23, Rue du Loess, BP 43, 67034 Strasbourg-Cedex 2, France*

Ultrafast magneto-optical (MO) experiments constitute a powerful tool to explore the magnetization dynamics of diverse materials. Over the last decade, there have been many theoretical and experimental developments on this subject. However, the relation between the magnetization dynamics and the transient MO response still remains unclear. In this work, we calculate the magnetization of a material, as well as the magneto-optical rotation and ellipticity angles measured in a single-beam experiment. Then, we compare the magnetization to the MO response. The magnetic material is modeled by a three-level Λ-type system, which represents a simple model to describe MO effects induced by an ultrafast laser pulse. Our calculations use the density matrix formalism, while the dynamics of the system is obtained by solving the Lindblad equation taking into account population relaxation and dephasing processes. Furthermore, we consider the Faraday rotation of the optical waves that simultaneously causes spin-flip. We show that the Faraday angles remain proportional to the magnetization only if the system has reached the equilibrium-state, and that this proportionality is directly related to the population and coherence decay rates. For the non-equilibrium situation, the previous proportionality relation is no longer valid. We show that our model is able to interpret some recent experimental results obtained in a single-pulse experiment. We further show that, after a critical pulse duration, the decrease of the ellipticity as a function of the absorbed energy is a characteristic of the system. © *2015 AIP Publishing LLC*.
[http://dx.doi.org/10.1063/1.4927841]

I. INTRODUCTION

Ultrafast demagnetization of ferromagnetic thin films by a femtosecond laser pulse[1] has been widely studied in recent years. It has been the starting point of numerous investigations on various magnetic materials,[2,3] in view of the potential uses of controlling spin dynamics using ultrashort light pulses. However, in spite of many studies on the subject, the mechanisms responsible for these effects have not been elucidated yet. In particular, those which are relevant during the initial phase of the dynamics. Understanding these mechanisms is of a fundamental interest, and that is why many proposals to explain this light-induced demagnetization have been proposed. In recent years, various spin-flip processes have been suggested, highlighting the role played by phonons,[4] magnons,[5] the spin-orbit coupling (SOC),[6–8] or the helicity transfer of the incident light.[9] Alternative studies propose the relativistic coupling between spins and photons, as a coherent process occurring during the propagation of the laser pulse.[10,11]

Besides the previous fundamental aspects, another problematic issue has recently appeared, concerning the question of whether or not the experimental time-resolved magneto-optical (MO) signal really reflects the magnetization dynamics on the subpicosecond time-scale.[12–16] An attempt to give a new insight to this question can be done by evaluating the appropriate magnetization change hidden in the measured

nonlinear magneto-optical rotation θ and ellipticity η in a single-pulse Faraday experiment. Such an experiment has already been performed by Bigot and co-workers,[10] and they have analyzed the nonlinear dependence of the rotation and of the ellipticity with respect to the absorbed energy. We emphasize that this experiment was initially interpreted assuming that a SOC involving the electric field of the laser pump could be added to that of the ionic static field at high laser intensities. Without rejecting this interpretation, the single-pulse Faraday experiment can be considered as an interesting tool to study the importance of physical parameters on the total induced rotation and ellipticity. As an example, a recent semi-classical model[17] has been proposed to indirectly estimate the part of magnetization change in nickel films, by comparing the available experimental data with a theoretical nonlinear Faraday phase mainly induced by a nonlinear charge perturbation.

In this work, we focus on the problematic of the magneto-optical measurements. The main goal of this paper is to compare the behavior of the magnetization with that of the rotation and ellipticity angles measured in a single-pulse Faraday experiment. The understanding of what is being measured in a single-beam experiment is a first step before attempting a description of a multiple-beam experiment. We have chosen to model the medium as a three-level Λ-type system. This represents the simplest model to describe the

magneto-optical effects induced by ultrafast laser pulses. Recently, Lefkidis and Hübner[18] have theoretically analyzed laser-induced spin-flip processes based on Λ-type systems. They have shown that their analytical results were consistent with those already obtained using numerical approaches on more realistic systems.[19] However, their model did not include phase or energy relaxation processes. We work in the density matrix formalism, where we take into account the population relaxation and dephasing by numerically solving the Lindblad equation of the Λ system excited by a laser pulse. We are able to calculate the system polarization and to specify how the induced magnetization change translates in the measurement of rotation and ellipticity. The latter quantities are determined by the modeling of experimental polarizing beam splitter (PBS) method. Since we are only concerned with the analysis of experimental signals, the damping rates will be phenomenologically described. It is beyond the scope of this work to give a complete understanding of the mechanisms underlying the ultrafast magnetic dynamics.

This paper is organized as follows. In Section II, we model a single-pulse Faraday experiment. The propagation equations of the electric field are solved in the slowly varying envelope approximation, and the medium polarization is obtained by solving the master equation for the density matrix. No assumptions are made concerning the exciting field intensity. Then, we determine the magneto-optical rotation and ellipticity measured with a PBS. Section III is devoted to the analysis of the correlations between the magnetization and the simulated experimental signals. In Section IV, we discuss the approximations of the model. We provide our conclusions in Section V.

II. THEORY

Our purpose is to theoretically describe a single-femtosecond-pulse Faraday experiment where the material is excited by a linearly polarized ultra-short laser pulse. As a consequence of the light-matter interaction, the polarization state of the incident light is modified, and the transmitted field acquires an elliptical state with a polarization characterized by a rotation and ellipticity angles. In the experiments, the transmitted field is analyzed with a half-wave plate (HWP) to characterize the magneto-optical rotation, and a quarter-wave plate (QWP) is added to measure the ellipticity. The light beam is then split into two orthogonally polarized components by a PBS, and the resulting intensities are measured by two photodiodes (Pd).[10,20,21] The experimental configuration is sketched in Fig. 1.
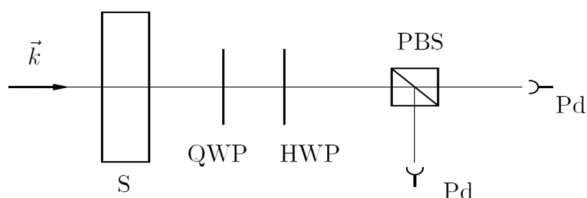
The laser field $E(z,t)$ can be expressed as

$$E(z,t) = \frac{1}{2}\mathcal{E}(z,t)e^{i(\omega t - kz)} + c.c., \tag{1}$$

where k and ω are, respectively, the wavenumber and the pulsation of the field, with c.c. standing for complex conjugate. The complex amplitude $\mathcal{E}(z,t)$ can be written under the form

$$\mathcal{E}(z,t) = \mathcal{E}_x(z,t)e_x + \mathcal{E}_y(z,t)e_y, \tag{2}$$

where e_x and e_y are two perpendicular unit vectors of the laboratory frame. By considering an experiment such as the one performed by Bigot and his coworkers,[10] we can assume that the thickness L of the system is much smaller than the wavelength of the laser field. As a consequence, we neglect the propagation effects over the medium. Therefore, writing the system polarization $P(z,t)$ and the magnetization $M(z,t)$ under the form

$$P(z,t) = \frac{1}{2}\mathcal{P}(z,t)e^{i(\omega t - kz)} + c.c., \tag{3}$$

and

$$M(z,t) = \frac{1}{2}\mathcal{M}(z,t)e^{i(\omega t - kz)} + c.c., \tag{4}$$

and using the slowly varying envelope approximation, the field components are written as[22]

$$\begin{cases} \mathcal{E}_x(L,t) = \mathcal{E}_x(0,t) - iL\frac{\mu_0\omega c}{2}\mathcal{P}_x(0,t) - iL\frac{\mu_0\omega}{2}\mathcal{M}_y(0,t) \\ \mathcal{E}_y(L,t) = \mathcal{E}_y(0,t) - iL\frac{\mu_0\omega c}{2}\mathcal{P}_y(0,t) + iL\frac{\mu_0\omega}{2}\mathcal{M}_x(0,t), \end{cases} \tag{5}$$

where c is the speed of light and μ_0 is the vacuum permeability. We have noted $\mathcal{P}_x(0,t)$ and $\mathcal{P}_y(0,t)$ the components of $\mathcal{P}(0,t)$ in the basis set (e_x, e_y). Similarly, the two components of the magnetization amplitude will be noted by $\mathcal{M}_x(0,t)$ and $\mathcal{M}_y(0,t)$.

In order to calculate the polarization and the magnetization, we need to model the excited material. Following Lefkidis and Hübner,[18] the active medium is described by a three-level system, as shown schematically in Fig. 2. It is assumed that the electric field couples only the states $|1\rangle$ and
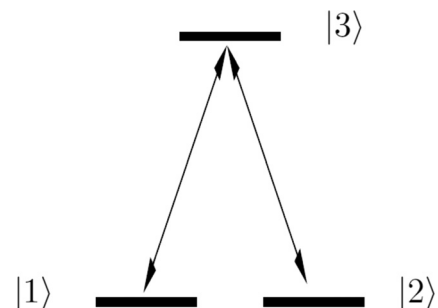

FIG. 1. Experimental configuration. S: sample; QWP: quarter-wave plate; HWP: half-wave plate; PBS: polarizing beam splitter; and Pd: photodiode.

FIG. 2. Λ-type scheme for the three-level system. Radiative transitions are only allowed between the states $|1\rangle$ and $|3\rangle$ and between the states $|2\rangle$ and $|3\rangle$.

$|3\rangle$, and the states $|2\rangle$ and $|3\rangle$. Dipole transitions between the states $|1\rangle$ and $|2\rangle$ are not allowed. Here, a system of two electrons is assumed and all the three states are spin triplets, ^3S and ^3P, where S and P correspond to $L=0$ and $L=1$, L being the quantum number associated to the orbital angular momentum. Due to the SOC, the good quantum numbers are j and m_j which are, respectively, related to the operator $\boldsymbol{J}^2$, where $\boldsymbol{J} = \boldsymbol{L} + \boldsymbol{S}$ is the total angular momentum, and to the operator J_z, the z-projection of $\boldsymbol{J}$. The ground state $|1\rangle$ corresponds to the spin-down of the S state and the second one $|2\rangle$ to the spin-up. In other words

$$\begin{aligned} |1\rangle &= |j=1, m_j=-1\rangle \\ &= |L=0, M_L=0; S=1, M_S=-1\rangle, \end{aligned}$$

and

$$\begin{aligned} |2\rangle &= |j=1, m_j=1\rangle \\ &= |L=0, M_L=0; S=1, M_S=1\rangle. \end{aligned}$$

The excited state state $|3\rangle$ corresponds to the ^3P state. As a consequence of the SOC, the states $^3P_0$, $^3P_1$, and $^3P_2$ in spectroscopic notation $^{2S+1}L_j$ are non-degenerate. Moreover, as only electric dipole transitions are considered here, the selection rules, $\Delta m_j = 0, \pm 1$, imply that the excited state is characterized by $m_j=0$. For convenience, and following Lefkidis's model,[18] the excited state $|3\rangle$ will be described by the $^3P_1$ state which can be written as

$$\begin{aligned} |3\rangle &= |j=1, m_j=0\rangle \\ &= \{|L=1, M_L=1; S=1, M_S=-1\rangle \\ &\quad - |L=1, M_L=-1; S=1, M_S=1\rangle\}/\sqrt{2}. \end{aligned}$$

In the basis set $\{|1\rangle, |2\rangle, |3\rangle\}$, the matrix representation of the unperturbed system Hamiltonian H_0 is given by

$$H_0 = \begin{pmatrix} E_g & & \\ & E_g & \\ & & E_e \end{pmatrix}, \qquad (6)$$

where E_g is the energy of the degenerate states $|1\rangle$ and $|2\rangle$, and E_e is the energy of the excited state $|3\rangle$. The interaction with the electric field $\boldsymbol{E}(z,t)$ is described in the electric dipole approximation by the system-field interaction Hamiltonian

$$H_{int}(z,t) = -\boldsymbol{\mu} \cdot \boldsymbol{E}(z,t), \qquad (7)$$

where the electric field $\boldsymbol{E}(z,t)$ is given by the relation (1). The dipole moment takes the form $\boldsymbol{\mu} = \mu_x \boldsymbol{e}_x + \mu_y \boldsymbol{e}_y$, where the matrix representations of μ_x and μ_y are given by[18]

$$\mu_x = 2\mu \begin{pmatrix} 0 & 0 & 1 \\ 0 & 0 & -1 \\ 1 & -1 & 0 \end{pmatrix} \quad \text{and} \quad \mu_y = 2\mu \begin{pmatrix} 0 & 0 & i \\ 0 & 0 & i \\ -i & -i & 0 \end{pmatrix}, \qquad (8)$$

with $4\mu = \langle L=0, M_L=0|x|p_x\rangle$, and $|p_x\rangle = (|L=1, M_L=1\rangle + |L=1, M_L=-1\rangle)/\sqrt{2}$. We stress that throughout our work, $\boldsymbol{\mu}$ represents the electric dipole moment (and not the magnetic moment).

It is straightforward to show that only the z component of the magnetic moment $\boldsymbol{M} = \frac{\mu_B}{\hbar}(\boldsymbol{L} + 2\boldsymbol{S})$ is non zero. Its matrix representation is given by

$$M_z = \begin{pmatrix} -2\mu_B & 0 & 0 \\ 0 & 2\mu_B & 0 \\ 0 & 0 & 0 \end{pmatrix}, \qquad (9)$$

where μ_B is the Bohr magneton. As a consequence, the relation (5) can be simplified to the form

$$\begin{cases} \mathcal{E}_x(L,t) = \mathcal{E}_x(0,t) - iL\dfrac{\mu_0 \omega c}{2}\mathcal{P}_x(0,t) \\ \mathcal{E}_y(L,t) = \mathcal{E}_y(0,t) - iL\dfrac{\mu_0 \omega c}{2}\mathcal{P}_y(0,t). \end{cases} \qquad (10)$$

Therefore, we only need to calculate the system polarization $\boldsymbol{P}(z,t)$, which is given by $\boldsymbol{P}(z,t) = \text{Tr}(\boldsymbol{\mu}\rho(z,t))$. We denote ρ the system density matrix and Tr the trace operation over the three-level system. In order to describe the dynamics of the system, we assume that the time evolution of ρ can be obtained from a Markovian master equation. The Liouville equation thus takes the form

$$\frac{d\rho}{dt} = -\frac{i}{\hbar}[H_0 + H_{int}(t), \rho] + \mathcal{L}_{\text{relax}}\rho, \qquad (11)$$

where $\mathcal{L}_{\text{relax}}$ is the Lindblad superoperator[23] defined by

$$\begin{aligned} \mathcal{L}_{\text{relax}}\rho &= \frac{\gamma_{31}}{2}(2\sigma_{13}\rho\sigma_{31} - \sigma_{33}\rho - \rho\sigma_{33}) \\ &\quad + \frac{\gamma_{32}}{2}(2\sigma_{23}\rho\sigma_{32} - \sigma_{33}\rho - \rho\sigma_{33}) \\ &\quad + \frac{\gamma_{21}}{2}(2\sigma_{12}\rho\sigma_{21} - \sigma_{22}\rho - \rho\sigma_{22}) \\ &\quad + \frac{\gamma_3}{2}(2\sigma_{33}\rho\sigma_{33} - \sigma_{33}\rho - \rho\sigma_{33}) \\ &\quad + \frac{\gamma_2}{2}(2\sigma_{22}\rho\sigma_{22} - \sigma_{22}\rho - \rho\sigma_{22}), \qquad (12) \end{aligned}$$

where $\sigma_{ij} = |i\rangle\langle j|$ stand for the projection operators, $(i,j = 1,2,3)$. The first three terms on the right-hand side of Eq. (12) describe dissipative processes with energy loss. We have noted γ_{ij} the rate of spontaneous emission from state $|i\rangle$ to state $|j\rangle$. The last two terms correspond to energy-conserving dephasing processes which are characterized by the rates γ_2 and γ_3. By using the Lindblad's representation, we do not make assumptions about the physical origin of the relaxation terms. Many microscopic mechanisms have been proposed as, for example, Elliot-Yaffet-like mechanisms based on electron-phonon,[24] electron-magnons,[25] electron-electron[26] scatterings, or superdiffusive transport.[27] All these processes affect the spin and contribute to the thermalization of the system resulting in a characteristic time related to the spontaneous population decay rate, which can be approximated by a thermalization time of the order of 100 fs. In addition, our model does not address the question of the physical nature of the reservoir, which supplies the angular momentum ensuring the conservation of the total angular momentum.[13,28] In our approach, the three-level system

interacts with a bath in such a way that the total energy and the total angular momentum of the system-bath-photons are conserved. The physical nature of the bath, and of its interaction with the three-level system, remains an open question which does not constitute the object of this work.

Equation (11) can be written under the form

$$\frac{d\rho}{dt} = \mathcal{L}(t)\rho, \tag{13}$$

where $\mathcal{L}(t)\rho = -\frac{i}{\hbar}[H_0 + H_{int}(t), \rho] + \mathcal{L}_{relax}\rho$. For short time-increments, Δt, we can approximate the propagator by[29]

$$\rho(t + \Delta t) = e^{\Delta t \mathcal{L}\left(t + \frac{\Delta t}{2}\right)}\rho(t), \tag{14}$$

and we then use the Cayley's representation[30] of the short-time propagator

$$e^{\Delta t \mathcal{L}} \simeq \left(1 - \frac{\Delta t}{2}\mathcal{L}\right)^{-1}\left(1 + \frac{\Delta t}{2}\mathcal{L}\right), \tag{15}$$

in order to calculate the density matrix. Thus, the polarization of the system can be evaluated and the electric field going out of the sample can be determined by using the relation (10) where, for convenience, the factor $L\mu_0\omega c/2$ has been set to unity.

We consider the usual experimental setup for magneto-optical measurements with a polarization bridge,[10,11,31] where the magneto-optical rotation is determined by analyzing the outgoing field with a half-wave plate tilted by an angle of $\pi/8$ with respect to the $\boldsymbol{e}_x$ axe. The Jones-matrix[31] of this half-wave plate is written as

$$\frac{1}{\sqrt{2}}\begin{pmatrix} 1 & 1 \\ 1 & -1 \end{pmatrix}, \tag{16}$$

enabling to evaluate the rotated field. In order to take into account of the integration time of the photodiodes, the field intensities I_x^θ and I_y^θ are obtained from

$$I_\alpha^\theta = \int_{-\infty}^{\infty} |\mathcal{E}_\alpha^\theta(t)|^2 dt; \quad \alpha = x, y, \tag{17}$$

where $\mathcal{E}_\alpha^\theta(t)$ denotes the complex amplitude of the α-component of the rotated field. Finally, the magneto-optical rotation θ is determined by

$$\theta = \frac{I_x^\theta - I_y^\theta}{I_x^\theta + I_y^\theta}. \tag{18}$$

Following a similar procedure, the magneto-optical ellipticity η can be measured by adding a quarter-wave plate to the previous half-wave plate. In this case, the total Jones matrix is given by

$$\frac{1}{2}\begin{pmatrix} 1 & -i \\ 1 & i \end{pmatrix}, \tag{19}$$

and the field intensities I_x^η and I_y^η can be calculated to determine the magneto-optical ellipticity

$$\eta = \frac{I_x^\eta - I_y^\eta}{I_x^\eta + I_y^\eta}. \tag{20}$$

Our main goal is to establish the correlation between θ (or η), and the magnetization of the system, which is given by

$$\langle M_z \rangle = 2\mu_B(\rho_{22} - \rho_{11}). \tag{21}$$

III. SIMULATIONS

For the purpose of this work, we assume that the exciting field is linearly polarized along the x-axis and, moreover, that its temporal envelope can be modeled by a square pulse expressed under the form

$$\mathcal{E}_x(0, t) = A[h(t) - h(t - \tau)]. \tag{22}$$

The function $h(t)$ stands for the Heaviside function, while A and τ are, respectively, the amplitude and the duration of the laser pulse. This assumption about the temporal dependence of the field envelope does not change the main physical conclusions and makes easier the analysis of our simulations because it simplifies some time behaviors due to the convolution of the field envelope and the system response.

A. Temporal analysis

We first start by considering an input pulse which is much longer than any characteristic times of the system dynamics. The dephasing times and the lifetimes are chosen to be 10 fs and 100 fs, respectively,[11] ($\gamma_{21} = \gamma_{32} = \gamma_{31} = 0.01\,\text{fs}^{-1}$ and $\gamma_2 = \gamma_3 = 0.1\,\text{fs}^{-1}$). These values have been used in a recent theoretical work describing coherent magneto-optics.[11] Even if they are arbitrary, they can describe realistic systems, since $1/\gamma_{ij}$ can refer to the thermalization time (≈ 100 fs) and $1/\gamma_i$ is usually a tenth of the latter. The energy difference $\hbar\omega_{eg} = E_e - E_g$ between the excited level $|3\rangle$ and the two degenerate levels $|1\rangle$ and $|2\rangle$ is fixed at $\hbar\omega_{eg} = 1.55\,\text{eV}$, which corresponds to a wavelength of 798 nm.[10] An analysis of the non-degenerate case ($E_1 \neq E_2$) is done in Section IV. We test our model by simulating the time evolution of the medium magnetization, represented in Fig. 3. Curves (a) and (b) in Fig. 3(I) correspond to a resonant excitation, while curves (c) and (d) are obtained in the non-resonant case with a resonance detuning of $\Delta\omega = \omega - \omega_{eg} = 0.025\omega_{eg}$. In the curves (a) and (c), we have arbitrarily set the field amplitude A to unity, while a strong field situation is depicted by the graphs (b) and (d) with a field amplitude seven times larger than the other cases. All the represented situations reach a plateau which depends on the system dynamics and tends to zero for a strong field amplitude. This last case corresponds to a population equilibrium between the states $|1\rangle$ and $|2\rangle$, and Rabi oscillations are observed in the temporal evolution of the magnetization. The plateau observed in these time evolutions is not surprising; it is due to the fact that the duration of the excitation is long enough with respect to the time scale for the system dynamics to reach a steady-state. We have set the pulse duration as 3 ps. It is important to note that these
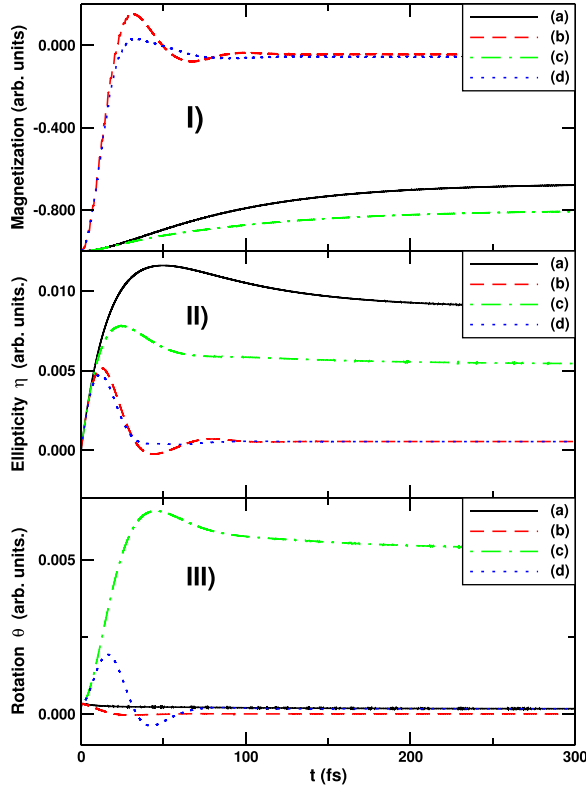
FIG. 3. MO response and magnetization. (I) Temporal evolution of the average value $\langle M_z \rangle$. (II) Temporal evolution of the ellipticity η. (III) Temporal evolution of the rotation θ. Curves (a) and (b) correspond to a resonant excitation, while curves (c) and (d) are obtained in the case of a non-resonant excitation. The field amplitude in curve (b) (respectively, (d)) is seven times greater than in curve (a) (respectively, (c)). The pulse duration has been chosen as 3 ps in all cases.

simulations show that the time demagnetization is a function of the system dynamics, of the field amplitude, and of the field envelope. As already mentioned, this latter is not properly taken into account in this work, since we used a simple square pulse model for the field envelope.

For convenience, in this part of the work, we have considered perfect photodiodes. The magneto-optical ellipticity $\eta(t)$ and the magneto-optical rotation $\theta(t)$ are then defined by the relations

$$\eta(t) = \frac{|\mathcal{E}_x^\eta(t)|^2 - |\mathcal{E}_y^\eta(t)|^2}{|\mathcal{E}_x^\eta(t)|^2 + |\mathcal{E}_y^\eta(t)|^2} \quad \text{and} \quad \theta(t) = \frac{|\mathcal{E}_x^\theta(t)|^2 - |\mathcal{E}_y^\theta(t)|^2}{|\mathcal{E}_x^\theta(t)|^2 + |\mathcal{E}_y^\theta(t)|^2},$$

$$(23)$$

where $\mathcal{E}_\alpha^\eta(t)$ and $\mathcal{E}_\alpha^\theta(t)$ (for $\alpha = x, y$) denote the complex amplitudes of the α–component of the fields detected in the ellipticity and the rotation measurement, respectively. In Figs. 3(II) and 3(III), we have represented $\eta(t)$ and $\theta(t)$ as functions of the time t. Due to the long duration of the excitation, all these curves reach again a steady-state value. We observe that for a high-field amplitude (curves (b) and (d) in Figs. 3(II) and 3(III)), the ellipticity and the rotation tend to zero. This is in agreement with the fact that for a strong field excitation, the population difference $\rho_{22} - \rho_{11}$ disappears. Curves (a) and (c) have been calculated with the same weak field amplitude but, as mentioned above, for different field

frequencies. We note that the corresponding plateau values of the ellipticity are of the same order, contrary to the plateau values of the rotation. This clearly appears in Fig. 3(III), where the values of the plateau of the curves (a) and (c) differ by one order of magnitude. This point can be easily understood by drawing in Fig. 4 the value of the plateau for both ellipticity and rotation as a function of the detuning resonance of the laser field, and for a field amplitude set to unity. We recover that the ellipticity and the rotation are related to the real and imaginary part of the refractive index. The variations represented in Fig. 4 explain why the rotation vanishes at the resonance and why the ellipticity is decreasing when the detuning of the laser frequency increases. For the non resonant situations considered in this work, we have chosen the frequency corresponding to the crossing-point where the ellipticity and the rotation are equal. This choice leads to signals of the same amplitude for weak field amplitude.

B. Steady-state behavior

The previous simulations enable us to analyze the steady-state behavior of the ellipticity and the rotation. In Figs. 5 and 6, we present the value of the plateau reached at long times by the ellipticity and the rotation, respectively, as a function of the field amplitude. Curves (a) and (c) stand for a resonant excitation, in contrast to curves (b) and (d), where a resonance detuning of $\Delta\omega = 0.025\omega_{eg}$ has been chosen. In order to analyze the influence of the system dynamics, the curves (a) and (b) have been calculated by setting $\gamma_{31} = \gamma_{32} = \gamma_{21} = 0.01 \text{ fs}^{-1}$ as the population relaxation rates, and $\gamma_2 = \gamma_3 = 0.1 \text{ fs}^{-1}$ as the coherence decay rates. In curves (c) and (d), the relaxation parameter values have been fixed to $\gamma_{31} = \gamma_{32} = \gamma_{21} = 0.03 \text{ fs}^{-1}$ and $\gamma_2 = \gamma_3 = 0.3 \text{ fs}^{-1}$. We have chosen a logarithmic scale for the x-axis in order to facilitate the comparison with experimental results.[10] We notice that the variations of the calculated curves are consistent with those observed in the experiment. For small amplitudes of the exciting field, the ellipticity and rotation are amplitude-independent, while they exhibit a monotonously decreasing behavior for stronger fields. These variations are
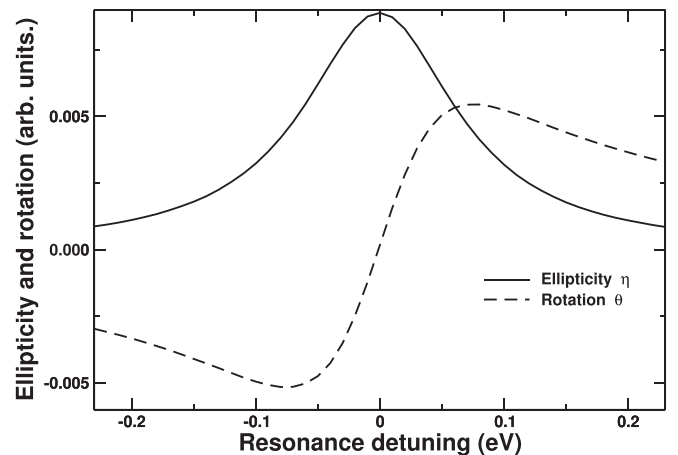

FIG. 4. Plateau value of the ellipticity and the rotation as a function of the resonance detuning. The field amplitude is set to unity.
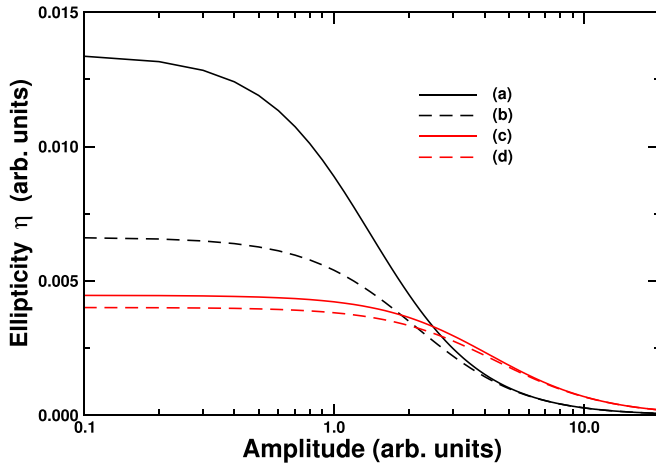
FIG. 5. Value of the plateau of the ellipticity as a function of the field amplitude. The cases (a) and (c) (solid lines) correspond to a resonant excitation, while curves (b) and (d) (dashed lines) represent a non-resonant excitation. The dynamic parameters for the black curves are: $\gamma_{31} = \gamma_{32} = \gamma_{21} = 0.01 \mathrm{fs}^{-1}$ and $\gamma_2 = \gamma_3 = 0.1 \mathrm{fs}^{-1}$. The values considered for the red curves are: $\gamma_{31} = \gamma_{32} = \gamma_{21} = 0.03 \, \mathrm{fs}^{-1}$ and $\gamma_2 = \gamma_3 = 0.3 \, \mathrm{fs}^{-1}$.

related to that of the system populations. The ellipticity and the rotation provide a signature of the difference of population between the states $|1\rangle$ and $|2\rangle$. From another standpoint, this population difference leads to a demagnetization of the system, as it can be seen on Fig. 7, where the value of the plateau reached by the magnetization at long times is presented as a function of the field amplitude. Given our choice of parameter values, for one set of coherence and population decay rates (black curves or red curves), the differences between the simulations calculated for a resonant excitation (solid lines) and the ones obtained in the non-resonant case (dashed lines) are not significant. Nevertheless, this difference decreases as the coherence decay rates increase.

The medium magnetization at long times depends of the field amplitude, as shown previously in Fig. 3(I), and it is also related to the system dynamics. This last point is recovered in Fig. 7, where the black and the red curves are clearly distinct, showing that the vanishing of the ellipticity and of the rotation for strong field amplitudes also depends on the system dynamics. Our calculations enable us to settle the
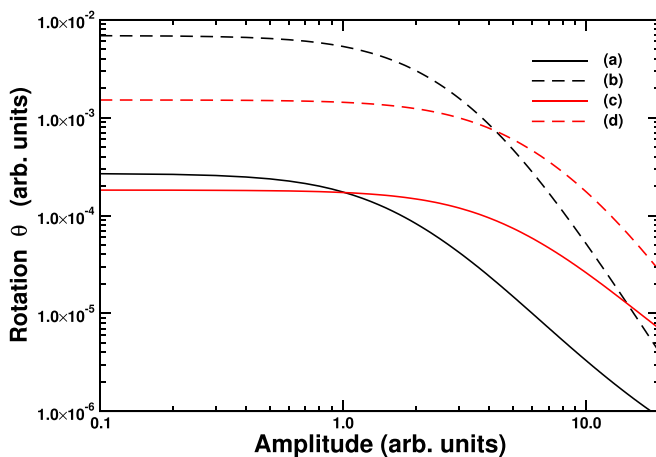
correlations between the magnetization and the ellipticity or the rotation measured in a single-pulse experiment. In particular, using the data of Figs. 5–7, we have plotted the ellipticity and the rotation as a function of the magnetization in Figs. 8 and 9.

We show in Fig. 8 that the steady-state values of the ellipticity and the rotation are proportional to the magnetization, and that this relation is directly related to the dynamics of the system. Indeed, the slopes of these straight lines depend on the population and coherence decay rates. We note the decrease of the slopes when the latter increase. The steady-state values of the ellipticity or of the magnetization can be analytically calculated, but they lead to involved expressions and are not simple functions of the system dynamics or of the field amplitude. Therefore, it is difficult to give a simple interpretation of the decrease of these slopes. These remarks are also valid for the magneto-optical rotation, as it can be seen in Fig. 9.

FIG. 7. Value of the magnetization plateau as a function of the field amplitude. All parameters are identical to those of Fig. 5.

FIG. 6. Value of the plateau of the rotation as a function of the field amplitude. All parameters are identical to those of Fig. 5.

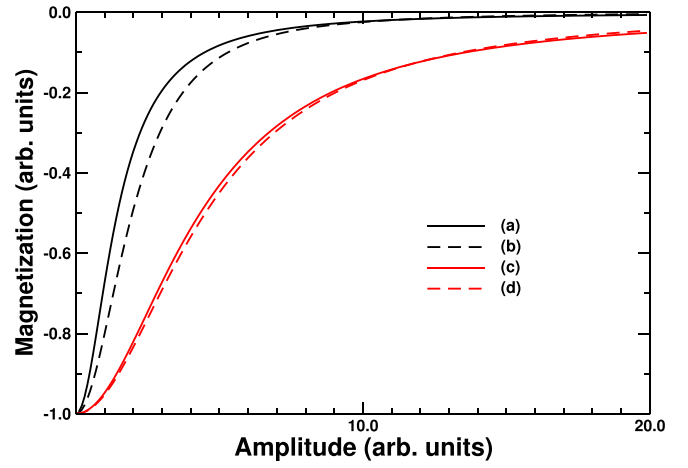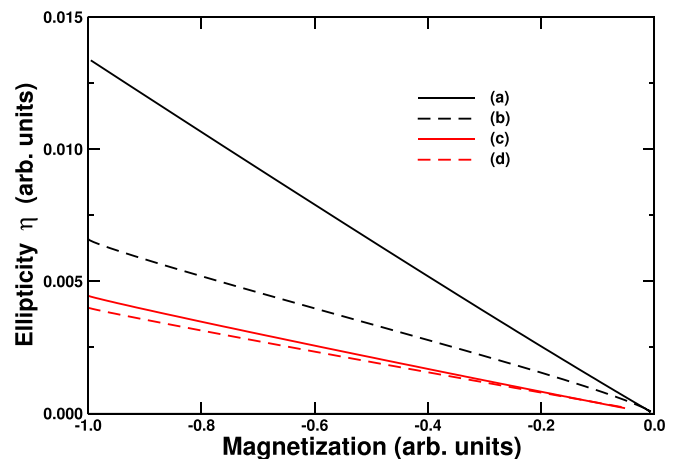FIG. 8. Value of the ellipticity plateau as a function of the average magnetization value $\langle M_z \rangle$. The cases (a) and (c) (solid lines) correspond to a resonant excitation, while curves (b) and (d) (dashed lines) represent a non-resonant excitation. The dynamic parameters for the black curves are: $\gamma_{31} = \gamma_{32} = \gamma_{21} = 0.01 \, \mathrm{fs}^{-1}$ and $\gamma_2 = \gamma_3 = 0.1 \, \mathrm{fs}^{-1}$, while the values taken for the red curves are: $\gamma_{31} = \gamma_{32} = \gamma_{21} = 0.03 \, \mathrm{fs}^{-1}$ and $\gamma_2 = \gamma_3 = 0.3 \, \mathrm{fs}^{-1}$.
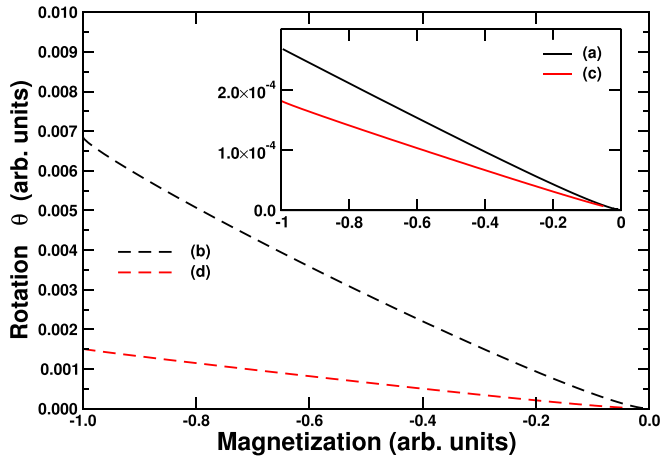
FIG. 9. Value of the rotation plateau as a function of the average value $\langle M_z \rangle$. The parameters are identical to those of Fig. 8.

C. Short-time response and influence of the pulse duration

In this last section, we consider a situation where the pulse duration is of the same order than the time evolution of the system dynamics. The magnetization illustrated in Fig. 3(I) shows that, in the case of short pulse excitation, the steady-state behavior will not be reached whatever be the field amplitude. This comment also applies to the ellipticity and the rotation presented in Figs. 3(II) and 3(III). If we compare Fig. 3(I-a) with Fig. 3(II-a), we note that, at short times, the magnetization increases monotonically in contrast with the ellipticity, which exhibits a maximum before decreasing and reaching the plateau at long times. In the Rabi regime, Figs. 3(I-b) and 3(II-b) show both an oscillation, but without an obvious phase relation among them. In other words, the analysis of these time variations points to the conclusion that for short times there is no simple relation between the magnetization and the ellipticity. The relation of proportionality previously found at long times no longer applies. This point has already been noted in the literature,[12–16] but in the present work we arrive at this conclusion by modeling the experimental signals.

Moreover, the ellipticity can be calculated even if its correlation with the magnetization is not clearly defined. In order to establish a more precise comparison with the experimental results, we plot in Fig. 10 the ellipticity as a function of the absorbed energy U_{abs}, which is proportional to the square of the field amplitude and to the pulse duration.[17,32] It must be noted that the ellipticity has been calculated following the relation (20), where the integration time of the detectors is taken into account. Figure 10 shows the ellipticity as a function of the absorbed energy for different pulse duration and for different dynamics parameters. Curves (a), (b), and (c) denote, respectively, a pulse duration of 200 fs, 100 fs, and 50 fs. The black curves correspond to $\gamma_3 = \gamma_2 = 0.1\,\mathrm{fs}^{-1}$ and the red ones to $\gamma_3 = \gamma_2 = 0.3\,\mathrm{fs}^{-1}$. The excitation is resonant and the values $\gamma_{31} = \gamma_{32} = \gamma_{21} = 0.01\,\mathrm{fs}^{-1}$ have been chosen. For the ease of reading, we only present the ellipticity, since as shown in Section III B, the rotation behavior is similar to that of the ellipticity. These variations are
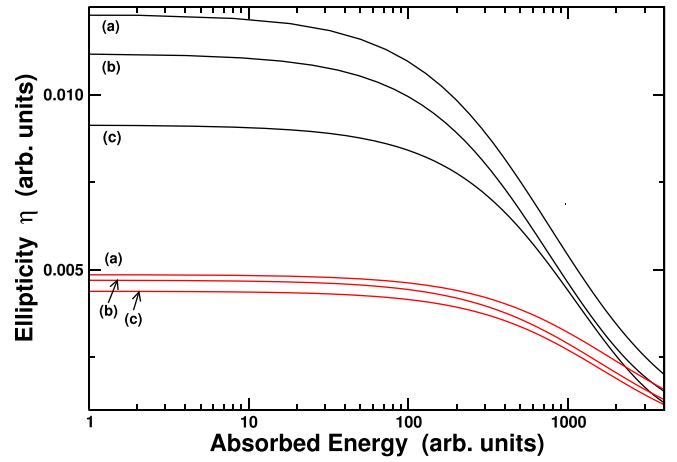

FIG. 10. Ellipticity as a function of the absorbed energy U_{abs}. Curves (a), (b), and (c) correspond, respectively, to a pulse duration of 200 fs, 100 fs, and 50 fs. For the black curves, we have fixed $\gamma_3 = \gamma_2 = 0.1\,\mathrm{fs}^{-1}$ and the values $\gamma_3 = \gamma_2 = 0.3\,\mathrm{fs}^{-1}$ have been chosen for the red ones.

consistent with the measured ellipticity in a single-pulse experiment[10] and show that our model can be used to interpret experimental results. In order to clearly illustrate the effect of the pulse duration, we did not normalize our results in contrast to what is usually done for experimental curves.

It is important to analyze whether the decrease of the ellipticity is a feature of the medium dynamics. Towards this goal, we considered the interval $U_{abs} \in [500, 1000]$, where all the calculated ellipticities are close to straight lines. In addition to the previous simulations presented in Fig. 10, we calculated the ellipticity as a function of the absorbed energy for other pulse durations ($\tau = 150\,\mathrm{fs}$, $\tau = 50\,\mathrm{fs}$, $\tau = 25\,\mathrm{fs}$, and $\tau = 15\,\mathrm{fs}$), and for other dynamical parameters ($\gamma_3 = 0.5\,\mathrm{fs}^{-1}$ and $\gamma_3 = 0.05\,\mathrm{fs}^{-1}$). The corresponding curves are not presented in this paper, but with this sample of 24 curves we have calculated the slope of each one in the interval $U_{abs} \in [500, 1000]$. The results are presented in Fig. 11, where we plot the slopes of the straight lines as a function of the pulse duration. The black, red, green, and blue curves correspond to $\gamma_3 = 0.05\,\mathrm{fs}^{-1}$, $0.1\,\mathrm{fs}^{-1}$, $0.3\,\mathrm{fs}^{-1}$, and $0.5\,\mathrm{fs}^{-1}$,
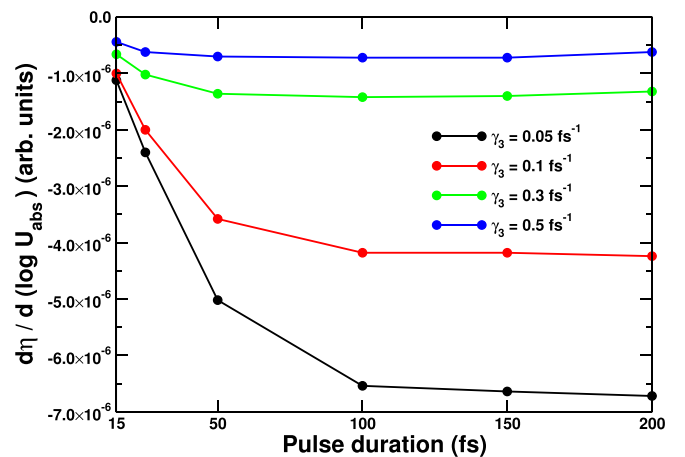

FIG. 11. Derivative of the ellipticity with respect to the logarithm of the absorbed energy as a function of the pulse duration. The slopes are calculated for $U_{abs} \in [500, 1000]$. The black, red, green, and blue curves correspond to $\gamma_3 = 0.05\,\mathrm{fs}^{-1}$, $0.1\,\mathrm{fs}^{-1}$, $0.3\,\mathrm{fs}^{-1}$, and $0.5\,\mathrm{fs}^{-1}$, respectively.

respectively. For each coherence decay rate γ_3, the calculated curves exhibit a similar behavior. We show that, after a critical pulse duration, the decrease of the ellipticity as a function of the absorbed energy does not depend any more on the pulse duration, and then, is a characteristic of the system. However, even in this latter case, the correlation between the magneto-optical ellipticity and the magnetization is not as simple as the one previously observed in the steady-state regime. Thus, a detailed study of the magnetization dynamics needs a theoretical description of a pump-probe experiment or an analysis of a four-wave mixing experiment. This latter can lead to a better understanding of the influence of dephasing processes, while a pump-probe can characterize the role of the population relaxation in the demagnetization process. These issues will be the subject of a future work.

IV. APPROXIMATIONS

It is important to make some comments about the approximations made in this work. They concern the use of a square pulse, the difference with the non-degenerate case, and the influence of the temperature.

As already mentioned, a square pulse has been used previously to model the time envelope of the pulse. Indeed, this assumption does not change our physical conclusions, but emphasizes the physical mechanisms which, in these conditions, are not convolved with the pulse envelope. To verify this point, we have considered a Gaussian pulse and our simulations show that for a duration much longer than any characteristic time of the system dynamics, the variations that we have presented in Fig. 5 or in Fig. 6 explain the time variations of the ellipticity or of the rotation calculated in this case. If we consider a pulse duration shorter, or of the same order than the time evolution of the system dynamics, we find again the results presented in Fig. 10. This behavior is not surprising, since the field intensities are calculated by a time integration to take into account the integration time of the photodiodes.

We would like to make some remarks on a situation where the initial and final states, $|1\rangle$ and $|2\rangle$, are non-degenerate. This situation should indeed be considered if the experiment is done on a ferromagnetic sample. It is important to note that from a point of view of physics, our previous results do not depend on the energy difference Δ between the states $|1\rangle$ and $|2\rangle$. Indeed, let us first consider a non-degenerate case, and let us assume that Δ is greater than the radiative width of these states. In this case, the $|2\rangle \rightarrow |3\rangle$ transition is not resonant and the steady-state populations can be analyzed by a simple kinetic model. In this work, we have assumed that $\gamma_{21} = \gamma_{32}$, hence, in the steady-state, there is no population difference between the states $|2\rangle$ and $|3\rangle$ independently of the value of Δ.

Let us consider now the degenerate case. There is no difference with the previous case, since the field absorption from the state $|2\rangle$ is balanced by the field-induced emission.

We can now consider a situation where $\gamma_{21} \neq \gamma_{32}$. In this case, we have a steady-state population difference between the states $|2\rangle$ and $|3\rangle$, but the coherence between these two states is very small provided that the $|2\rangle \rightarrow |3\rangle$ transition is

non resonant. Therefore, this situation is quite similar with the non-degenerate previous case where $\gamma_{21} = \gamma_{32}$. The magnetization will be different than before but the ellipticity will be the same. The variations described in Fig. 8 still remain valid, and the only changes are on the slopes of the straight lines. This situation does not depend on Δ if the $|2\rangle \rightarrow |3\rangle$ transition is non resonant. If we consider the resonant case, in contrast to the situation where $\gamma_{21} = \gamma_{32}$, there is now a coherence between the states $|2\rangle$ and $|3\rangle$ and the ellipticity decreases with respect to the non-degenerate case, but the magnetization remains. It must be noted that this situation can be induced from the non-degenerate case by a shift of the levels due to AC Stark effect,[33–36] and ellipticity variations should be observed.

Finally, we remark that Lefkidis and Hübner[18] have also analyzed the influence of the temperature in their model. They have shown that the induced material polarization averaged over a thermal distribution becomes weaker, but it does not disappear. As a consequence, the measured signal in an experiment does not vanish for finite temperatures.

V. CONCLUSION

We have investigated the relation between the magnetization and the MO response of a magnetic material after interaction with a short laser pulse. One of the goals of this work was to specify the role of the system dynamics. Towards this end, we have calculated the rotation and ellipticity angles in a single-femtosecond-pulse Faraday experiment, where the medium is modeled by a three-level Λ system, including population relaxation and dephasing processes. This system is a basic model which can lead to magneto-optical effects. Contrary to a pump-probe experiment, our work considers the Faraday rotation of the optical waves that simultaneously causes spin flip. By solving numerically the Lindblad equation, we calculate the MO response and the magnetization of the system.

We first have considered the steady-state regime where the pulse duration is much larger than any characteristic time of the system dynamics. By analyzing the steady-state values of the magnetization, the magneto-optical rotation, and ellipticity as a function of the field amplitudes, we have established that these quantities are directly related to the population of the system. We have retrieved that the MO response is proportional to the medium magnetization, and we have shown that the constant of proportionality is directly related to the population and coherence decay rates. We have shown that this constant of proportionality decreases when the latter increase.

We have then considered a non-equilibrium situation where the duration of the light pulse is shorter, or of the same order, as the time evolution of the system dynamics. In this case, the proportionality relation between the magnetization and the MO response no longer holds. Our theoretical model recovers the shape of a recent experimental study performed on a single-Faraday experiment which has measured the ellipticity angle as a function of the absorbed energy.[10] The dependence of the MO response with respect to the loss of coherences, and with respect to the pulse duration, is

clearly shown. On the other hand, we observe that, after a critical pulse duration, the decrease of the ellipticity as a function of the absorbed energy becomes independent of the pulse duration and can then be used to characterize the system.

ACKNOWLEDGMENTS

[1]E. Beaurepaire, J.-C. Merle, A. Daunois, and J.-Y. Bigot, Phys. Rev. Lett. **76**, 4250 (1996).

[2]A. Kirilyuk, A. V. Kimel, and T. Rasing, Rev. Mod. Phys. **82**, 2731 (2010).

[3]J.-Y. Bigot and M. Vomir, Ann. Phys. (Berlin) **525**, 2 (2013).

[4]B. Koopmans, G. Malinowski, F. D. Longa, D. Steiauf, M. Fähnle, T. Roth, M. Cinchetti, and M. Aeschlimann, Nat. Mater. **9**, 259 (2010).

[5]M. Lisowski, P. A. Loukakos, A. Melnikov, I. Radu, L. Ungureanu, M. Wolf, and U. Bovensiepen, Phys. Rev. Lett. **95**, 137402 (2005).

[6]W. Hübner and G. P. Zhang, Phys. Rev. B **58**, R5920(R) (1998).

[7]W. Hübner and G. P. Zhang, Phys. Rev. Lett. **85**, 3025 (2000).

[8]C. Boeglin, E. Beaurepaire, V. Halté, V. Lopez-Flores, C. Stamm, N. Pontius, H. Dürr, and J. Y. Bigot, Nature **465**, 458 (2010).

[9]G. Lefkidis, G. P. Zhang, and W. Hübner, Phys. Rev. B **87**, 014404 (2009).

[10]J.-Y. Bigot, M. Vomir, and E. Beaurepaire, Nat. Phys. **5**, 515 (2009).

[11]H. Vonesch and J.-Y. Bigot, Phys. Rev. B **85**, 180407(R) (2012).

[12]B. Koopmans, M. van Kampen, J. T. Kohlhepp, and W. J. M. de Jonge, Phys. Rev. Lett. **85**, 844 (2000).

[13]B. Koopmans, M. van Kampen, and W. J. M. de Jonge, J. Phys.: Condens. Matter **15**, S723 (2003).

[14]G. P. Zhang, W. Hübner, G. Lefkidis, Y. Bai, and T. F. George, Nat. Phys. **5**, 499 (2009).

[15]K. Carva, M. Battiato, and P. M. Oppeneer, Nat. Phys. **7**, 665 (2011).

[16]P. M. Oppeneer and A. Liebsch, J. Phys.: Condens. Matter **16**, 5519 (2004).

[17]Y. Hinschberger and P.-A. Hervieux, Phys. Rev. B **88**, 134413 (2013).

[18]G. Lefkidis and W. Hübner, Phys. Rev. B **87**, 014404 (2013).

[19]G. Lefkidis, G. P. Zhang, and W. Hübner, Phys. Rev. Lett. **103**, 217401 (2009).

[20]Z. Q. Qiu and S. D. Bader, Rev. Sci. Instrum. **71**, 1243 (2000).

[21]A. D. Slepkov, F. A. Hegmann, Y. Zhao, R. R. Tykwinski, and K. Kamada, J. Chem. Phys. **116**, 3834 (2002).

[22]R. Fleischhaker and J. Evers, e-print arXiv:0906.5301 [quant-ph].

[23]G. Lindblad, Commun. Math. Phys. **48**, 119 (1976).

[24]B. Koopmans, J. J. M. Ruigrok, F. D. Longa, and W. J. M. de Jonge, Phys. Rev. Lett. **95**, 267207 (2005).

[25]E. Carpene, E. Mancini, C. Dallera, M. Brenna, E. Puppin, and S. D. Silvestri, Phys. Rev. B **78**, 174422 (2008).

[26]M. Krauß, T. Roth, S. Alebrand, D. Steil, M. Cinchetti, M. Aeschlimann, and H. C. Schneider, Phys. Rev. B **80**, 180407(R) (2009).

[27]M. Battiato, K. Carva, and P. M. Oppeneer, Phys. Rev. Lett. **105**, 027203 (2010).

[28]S. R. Woodford, Phys. Rev. B **79**, 212412 (2009).

[29]A. D. Bandrauk and H. Shen, J. Chem. Phys. **99**, 1185 (1993).

[30]W. H. Press, B. P. Flannery, S. A. Teukolsky, and W. T. Vetterling, *Numerical Recipes in Fortran 77: The Art of Scientific Computing* (Cambridge University Press, Cambridge, 1992).

[31]D. Kliger, J. Lewis, and C. Randall, *Polarized Light in Optics and Spectroscopy* (Academic Press, 1990).

[32]G. Manfredi and P.-A. Hervieux, Opt. Lett. **30**, 3090 (2005).

[33]J. P. Barrat and C. Cohen-Tannoudji, J. Phys. Radium **22**, 329 (1961).

[34]A. Kaplan, M. F. Andersen, and N. Davidson, Phys. Rev. A **66**, 045401 (2002).

[35]R. Grimm, M. Weidemuller, and Y. B. Ovchinnikov, Adv. At., Mol., Opt. Phys. **42**, 95 (2000).

[36]J. B. Chen, F. Z. Wang, D. H. Yang, and Y. Q. Wang, Chin. Phys. Lett. **18**, 202 (2001).